

The Breakthrough Listen Search for Intelligent Life: Searching for Technosignatures in Observations of TESS Targets of Interest

Raffy Traas ^{1,2} , Steve Croft^{2,3}, Vishal Gajjar², Howard Isaacson^{2,4}, Matt Lebofsky², David H. E. MacMahon², Karen Perez⁵, Danny C. Price^{2,6}, Sofia Sheikh^{2,7}, Andrew P. V. Siemion^{2,3,8,9}, Shane Smith¹⁰, Jamie Drew¹¹, and S. Pete Worden¹¹

Department of Physics, University of Wisconsin—La Crosse, 1725 State Street, La Crosse, WI 54601, USA; traas5694@uwlax.edu, raffytraas14@gmail.com

Department of Astronomy, University of California Berkeley, Berkeley, CA 94720, USA

SETI Institute, Mountain View, CA, USA

4 University of Southern Queensland, Toowoomba, QLD 4350, Australia

Department of Astronomy, Columbia University, 550 West 120th Street, New York, NY 10027, USA

Centre for Astrophysics & Supercomputing, Swinburne University of Technology, Hawthorn, VIC 3122, Australia

Department of Astronomy and Astrophysics, Pennsylvania State University, University Park, PA 16802, USA

Department of Astrophysics/IMAPP, Radboud University, Nijmegen, Netherlands

University of Malta, Institute of Space Sciences and Astronomy, Malta

Hillsdale College, 33 E. College Street, Hillsdale, MI 49242, USA

Hillsdale College, 33 E. College Street, Hillsdale, MI 49242, USA

The Breakthrough Initiatives, NASA Research Park, Boulevard 18, Moffett Field, CA, 94035, USA

Received 2021 January 26; revised 2021 March 29; accepted 2021 April 7; published 2021 May 26

Abstract

Exoplanetary systems are prime targets for the Search for Extraterrestrial Intelligence (SETI). With the recent uptick in the identification of candidate and confirmed exoplanets through the work of missions like the Transiting Exoplanet Survey Satellite (TESS), we are beginning to understand that Earth-like planets are common. In this work, we extend the Breakthrough Listen (BL) search for extraterrestrial intelligence to include targeted searches of stars identified by TESS as potential exoplanet hosts. We report on 113 30 minute cadence observations collected for 28 targets selected from the TESS Input Catalog from among those identified as containing signatures of transiting planets. The targets were searched for narrowband signals from 1 to 11 GHz using the turboSETI pipeline architecture modified for compatibility with the Google Cloud environment. Data were searched for drift rates of $\pm 4\,\mathrm{Hz\,s^{-1}}$ above a minimum signal-to-noise threshold of 10, following the parameters of previous searches conducted by Price et al. and Enriquez et al. The observations presented in this work establish some of the deepest limits to date over such a wide band (1–11 GHz) for life beyond Earth. We determine that fewer than 12.72% of the observed targets possess transmitters operating at these frequencies with an equivalent isotropic radiated power greater than our derived threshold of $4.9 \times 10^{14}\,\mathrm{W}$.

Unified Astronomy Thesaurus concepts: Exoplanets (498); Technosignatures (2128); Search for extraterrestrial intelligence (2127)

1. Introduction

1.1. SETI Methods

The Search for Extraterrestrial Intelligence (SETI) is the endeavor to discover the existence of intelligent life elsewhere in the universe—one of the longest standing unanswered questions in science. There are three traditional techniques to detect intelligent life. The first method is in situ sampling, where studies are conducted at the site of interest. While this approach would provide us with results containing the least amount of uncertainty, it is infeasible in practice when studying extrasolar objects due to the vast interstellar distances involved. This brings about the need for techniques that can indirectly study sites of interest, which motivates the remaining two strategies: remote biosignature and technosignature searches. Technosignature searches are concerned with the detection of evidence of a technologically sophisticated civilization through their city lights, atmospheric pollution, satellites, powerful transmitters, etc. Traditionally, the majority of technosignature studies search for radio wave transmissions (Cocconi & Morrison 1959) typically in the 1-10 GHz frequency range. Biosignature searches use spectroscopy to detect planets with atmospheres or surfaces suitable for hosting life. This method is capable of detecting the presence of organic compounds in

planetary atmospheres and surfaces, thus indicating the possibility of life; however, it is challenging to unequivocally determine if those compounds derive from the emissions of living organisms or byproducts of inorganic processes. More importantly, in the case that a biosignature search indisputably detects the presence of life, it remains uncertain as to whether these organisms are complex, or even technological. In this regard, technosignature searches can be seen as a more holistic approach than biosignatures because, in principle, the detection of a technosignature would imply the existence of life. Moreover, whereas even the next generation of telescopes will only be able to probe nearby stars for biosignatures, searching for technosignatures allows the search to extend out to a much larger number of stars.

1.2. Breakthrough Listen

Breakthrough Listen (BL; Worden et al. 2017) is a ten-year initiative purposed toward the detection of technosignatures. Launched in 2015, it is equipped with the most capable tools and resources with which to conduct a SETI search, and constitutes the most comprehensive search to date (Enriquez et al. 2017; Price et al. 2020). BL conducts searches at optical wavelengths as well by using facilities such as the Automated Planet Finder to search for laser emission lines present in stellar

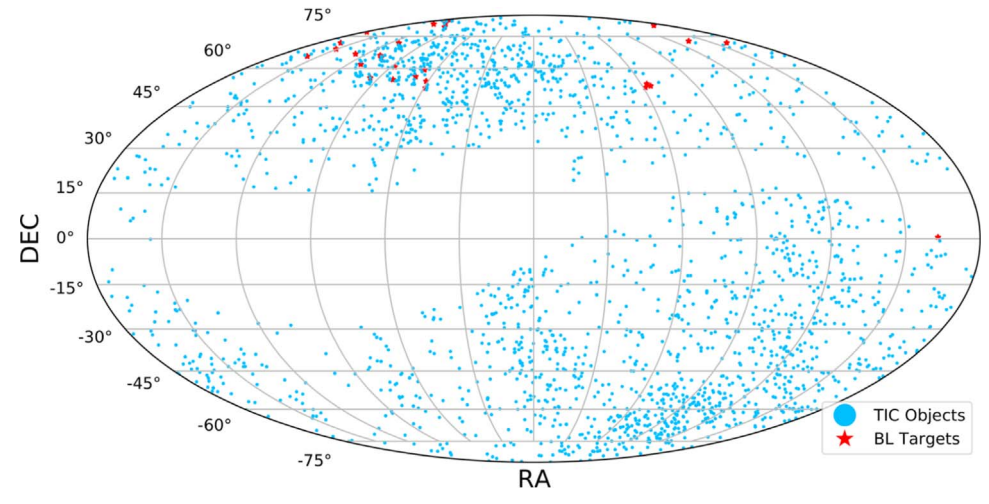


Figure 1. Distribution of BL targets analyzed in this paper, and a subset of existing TIC sources with associated TOI objects in equatorial coordinates. The subset was collected from resources provided by ExoFOP-TESS. The TESS project uses an all-sky survey approach to find transiting exoplanets.

spectra (Lipman et al. 2019), and the Very Energetic Radiation Imaging Telescope Array System (VERITAS) telescope to look for nanosecond optical pulses.

1.3. Exoplanets

Exoplanets are promising locations to search for technosignatures (e.g., Tingay et al. 2018; Tremblay & Tingay 2020). Earth harbors intelligent life and is itself an exoplanet from an extrasolar perspective, and this naturally leads us to presume the possibility of life having emerged in a similar environment. Besides an exoplanet residing within the habitable zone of its host star, we are more likely to assume it might harbor intelligent life if its properties are similar to that of Earth's. In the case that intelligent life eventually develops on these other worlds and become at least as technologically advanced as ourselves, they might possess some type of radio wave transmitting system, which forms the basis for many of our own telecommunications networks. Should such civilizations exist, we should be able to detect their presence as their signals inevitably spill out into space. While BL has performed searches of specific exoplanet systems (e.g., Perez et al. 2020; Sheikh et al. 2020), observing a larger sample can provide a limit on the number of nearby exoplanets on which radio transmitters aim signals directly toward Earth or output a sufficient amount of isotropic power to be detectable.

With the current surge in exoplanet discovery work being made by the NASA Transiting Exoplanet Survey Satellite (TESS), the number of confirmed exoplanets has increased dramatically alongside the number of stars identified as having signatures of transiting planet candidates, making a technosignature search of these objects particularly timely. Objects in the TESS Input Catalog (TIC), assembled from several existing catalogs as detailed by Stassun et al. (2019), are observed by TESS, and those identified as having signatures of transiting planets are subsequently registered into the TESS Objects of Interest (TOI) catalog—a list of TIC targets marked for follow-up observation. The recent completion of the TESS primary mission has found 66 confirmed exoplanets and 2120 targets of interest. ¹²

Table 1
Observation Parameters

Receiver	Frequency (GHz)	T _{sys} (K)	SEFD (Jy)	10σ Mini- mum Flux Density (Jy)	10σ Mini- mum EIRP (10 ¹² W)
S Band C Band	1.80–2.80 4.00–7.80	14.80 21.50	7.32896 10.6468	5.032 7.310	491.6 466.4 677.5 970.5

A collaboration between BL and scientists working on the TESS mission has initiated the search for extraterrestrial intelligence (ETI) in TESS target candidates. Removing those listed as false positives, BL observes objects present in the TOI catalog using the Exoplanet Follow-up Observing Program for TESS (ExoFOP-TESS¹³). The Robert C. Byrd Green Bank Observatory (hereafter GBT), a BL facility, observes targets above a decl. of -20° , resulting in an observation queue of 964 objects. The 28 targets included in this work are those that, to date, have been observed at all four of L, S, C, and X bands with the GBT, and are presented in Figure 1. This work searches more targets across 1–11 GHz than any previous BL search (e.g., Enriquez et al. 2018). A summary of the targets is given in Appendix B, from which the information included is sourced from the ExoFOP-TESS.

BL maintains a nonprescriptive approach to the targets it observes (see, e.g., Isaacson et al. 2017; Gajjar et al. 2020; Lacki et al. 2020). Although planetary systems are common, this sample adds significant value by extending the search to planetary systems with known transiting exoplanets.

Planetary systems are common, with the most common stars in the universe estimated to host several planets each (Hsu et al. 2020). Given this fact, we should be clear that these TOI systems are not interesting solely because they host planets; they are interesting because of the unique relative geometry that a transiting planet implies (Sheikh 2020). If TESS discovers a transiting planet, then Earth is necessarily in the ecliptic of that

¹² https://tess.mit.edu/publications/

¹³ https://exofop.ipac.caltech.edu/tess/view_toi.php

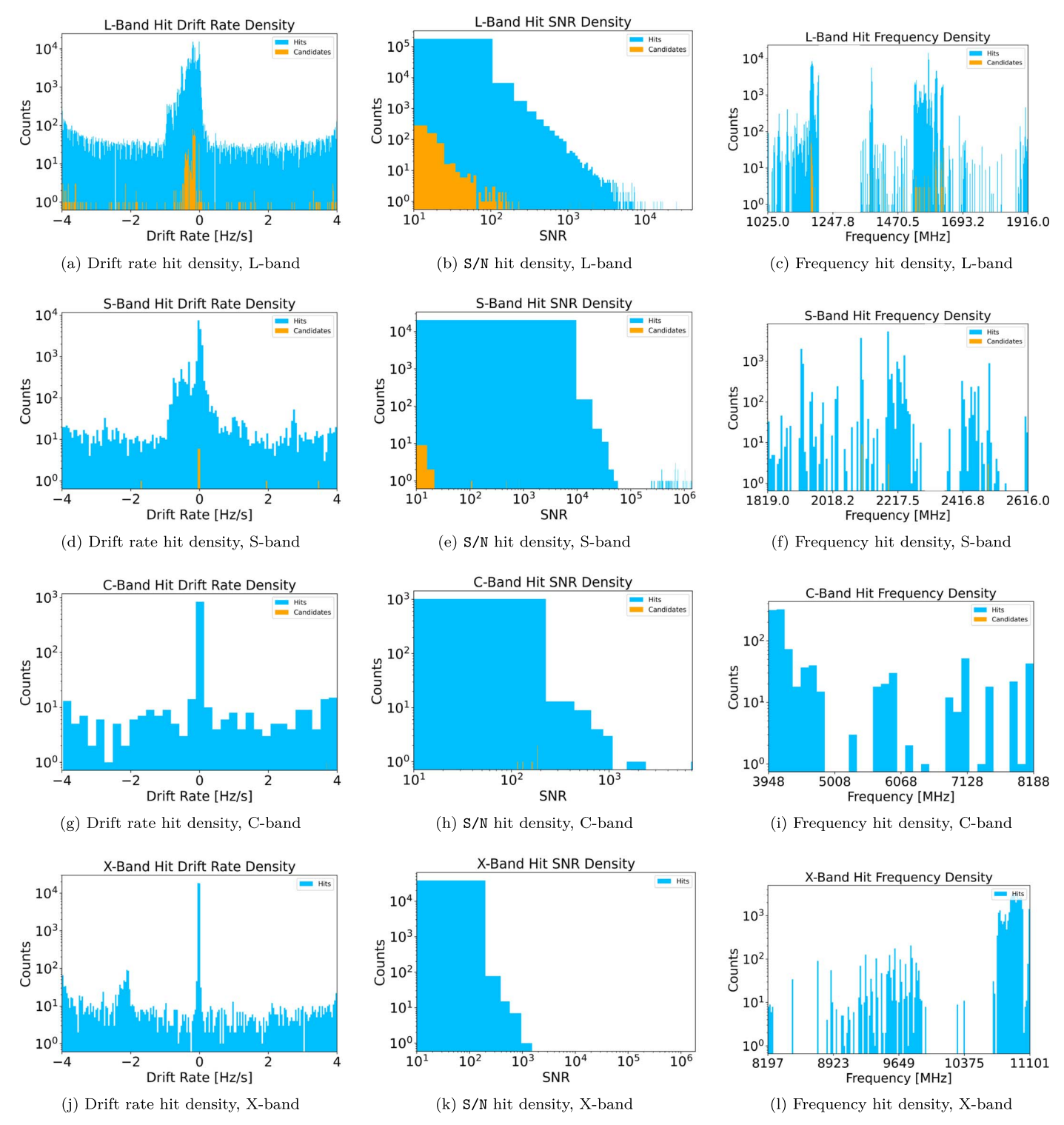


Figure 2. Histograms of the drift rate, S/N, and frequency density of the hits (blue) and candidates (orange). Note Figures 2(j), (k), and (l) reflect no candidates being found at the X band.

planetary system. This geometry leads to a higher likelihood of observing both intentional (beacon) technosignatures and unintentional (leakage) technosignatures from that system. For example, an ETI may preferentially send beacons along its ecliptic, knowing that its presence is most easily detected in that region of their sky due to their transit. Alternatively, the ETI may have similar interplanetary assets to those on Earth (e.g., radar to track asteroids in their system, spacecraft on or around other

bodies in their planetary system), which would likely be distributed along the ecliptic; strong radio leakage may be produced preferentially in the ecliptic due to these activities. Finally, an ETI that has settled multiple bodies in the same system would likely have strong and frequent communications between them. Again, we would expect these communications to be roughly aligned with the ecliptic, increasing the possibility that we pick up spillover radio transmissions on Earth.

Table 2
Candidates Found Across All Bands

Receiver	No. Cadences	Hours	No. Hits	No. Events	No. Candidates	TFM	Transmitter Limit ^a
\overline{L}	28	14.5	189321	34727	630	1995	12.72%
S	28	14.5	20673	5485	15	2038	12.72%
C	28	14.5	1054	269	6	1878	12.72%
X	29 ^b	14.5	38484	2794	0	4675	12.72%
Total	113	58.0	249532	43275	651	1072	12.72%

Notes.

2. Observations

Observations were conducted using the 100 m dish of the GBT and were recorded in an ABACAD cadence following the previous searches of Enriquez et al. (2017) and Price et al. (2020) in which each observation of a primary ("ON") target is alternated with observations of secondary ("OFF") targets. Each observation has a 5 minute duration, amounting to 30 minutes for a full cadence of 6 observations, for a total of over 3390 minutes on the sky. Data are recorded in accordance with the standard BL strategy detailed by Lebofsky et al. (2019). Details of the receivers are listed in Table 1.

3. Analysis

3.1. De-Doppler Pipeline

The fine-frequency resolution data products, with a channelization of 2.7 Hz (Lebofsky et al. 2019), amounting to a total of 24 TB, were analyzed for the presence of narrowband drifting signals using the turboSETI¹⁴ (Enriquez et al. 2017; Enriquez & Price 2019) pipeline. The data sets analyzed are available from the BL Open Data Archive.¹⁵

TurboSETI is a Doppler drift search algorithm designed to search for narrowband drifting signals. Detecting narrowband signals in regions crowded with radio frequency interference (RFI), and over wide ranges of Doppler drift rates, is challenging (see, e.g., Margot et al. 2021). Detection efficiencies for certain kinds of signals may be lower than expected, including for signals that are more complex than the simple assumption of a narrowband tone, and for signals with high drift rates. Minimum flux densities presented in Table 1 are for a simple low-drift-rate tone. Work is ongoing to enhance the capabilities of turboSETI, including better handling of signals spread across multiple frequency channels, and quantifying detection efficiency using signal injection and recovery. ¹⁶ In addition, we are exploring approaches, including machine learning (Brzycki et al. 2020), that offer improved performance in regions crowded with RFI. Nevertheless, turboSETI successfully finds the Voyager 1 spacecraft (an extraterrestrial transmitter that is a good stand-in for a real technosignature) in a blind search, ¹⁷ and can be used to place useful limits on the prevalence of technosignatures in the data set presented here.

Table 3
Summary Statistics

	L Band (%)	S Band (%)	C Band (%)	X Band (%)	Overall (%)
Hits	76	8	1	15	100
Events	80	13	1	6	100
Candidates	97	2	1	0	100
$Hit \rightarrow Event$	18	27	28	7	17
$Event \rightarrow Candidate$	2	0.27	2	0	2
$Hit \rightarrow Candidate$	0.33	0.07	0.57	0	0.26

Table 4 Event Groups

Receiver	Nevent groups	N _{single sources}	$N_{\text{non-RFI}}$
L Band	135	20	0
S Band	2	0	0
C Band	1	0	0
X Band	0	0	0

Prior to this work, the BL Doppler search pipeline was executed on the compute nodes at the UC Berkeley Data Center, where data to be processed was stored on disk. This work is the result of an endeavor to migrate the turboSETI pipeline onto the Google Cloud Platform (GCP). Data were stored in a Google Cloud Storage (GCS) Bucket, which was mounted to the file storage systems of each GCP Compute Engine to perform the analysis. Each of the 20 instances were installed with a containerized version of turboSETI as a *Docker* (Merkel 2014) image. ¹⁸ This process is shown in Appendix A. In this manner, turboSETI ran on a total of 113 full cadences, finding 249532 hits over a total of 696 individual observations. Only complete, six-target cadence sets were analyzed.

Narrowband drifting signals with a signal-to-noise ratio (S/N) > 10 detected by turboSETI are referred to as hits. A set of hits present in all "ON" observations falling within the range of frequencies subtended by a signal with constant drift are grouped into an event. That is, the nth event ε_n can be defined by Equation (1), where $t_{\rm obs}$ is the duration of each observation (5 minutes), ν_h is the frequency of a hit h present in the kth "ON" observation, and ν_0 and $\dot{\nu}_0$ are the frequency and drift

^a The limit on the existence of putative transmitters. Indicates the percentage of observed stars that possess transmitters above the EIRP_{min} threshold. That is, of the stars observed at a particular band, the transmitter limit is the maximum proportion of those which possess narrowband transmitters. Values were computed using a one-sided Poisson confidence interval, given a 50% probability of observing a signal if present.

^b There were two cadences of observations performed for TIC232967666.

¹⁴ https://github.com/UCBerkeleySETI/turbo_seti

¹⁵ http://seti.berkeley.edu/opendata

¹⁶ https://github.com/krishnabhattaram/TurboSETIRetrieval

¹⁷ https://github.com/elanlavie/VoyagerTutorialRepository

 $[\]overline{\ }^{18}$ The DOCKER image used in this work can be found here: https://hub.docker.com/r/rtraas/turbo-cloud

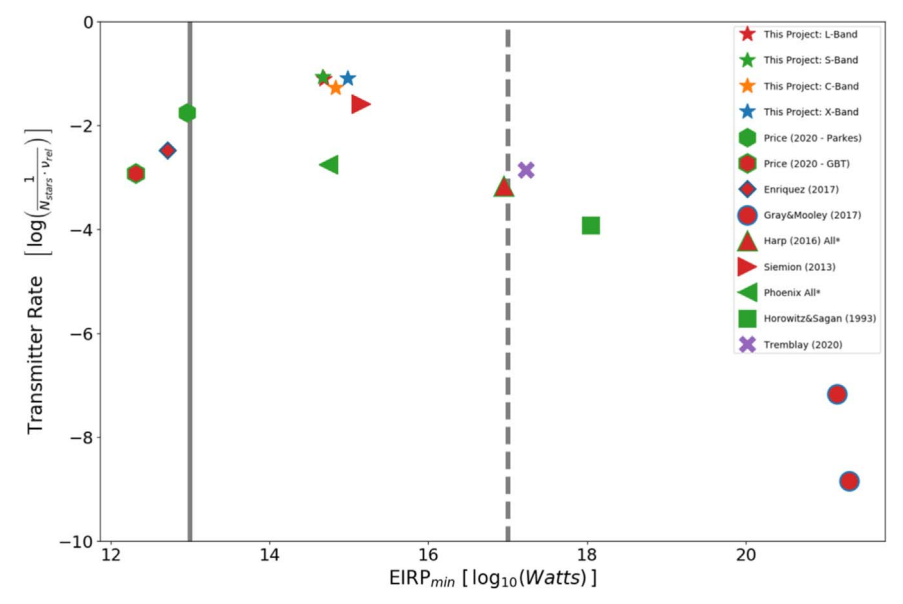


Figure 3. A comparison of the derived transmitter rate limits of this work with previous surveys, where red, green, orange, and blue correspond to searches conducted at the *L*, *S*, *C*, and *X* bands, respectively. Respectively, the vertical solid and dashed lines represent the equivalent isotropic radiated power (EIRP) of the Arecibo planetary radar, and the total solar power incident on Earth. Note that the Tremblay & Tingay (2020) data point represents a survey conducted at 113 MHz with the Murchison Widefield Array (MWA). The values for Project Phoenix are from Price et al. (2020). The Horowitz & Sagan (1993) data point represents an all-sky search near the 1420 MHz neutral hydrogen line, while Gray & Mooley (2017) searched the same line with the Very Large Array (VLA). Harp et al. (2016) conducted a search from 1–9 GHz with the Allen Telescope Array (ATA).

rate, respectively, of a hit present in the first "ON" observation A_0 in the cadence ABACAD or ABABAB. Events that contain no hits in all "OFF" observations are defined as potential candidates. Thus, the *n*th potential candidate ρ_n can be defined by Equation (2).

$$\varepsilon_{n} = \{ h \in A_{k} \colon \nu_{0} - \nu_{0} \cdot t_{\text{obs}} \leqslant \nu_{h} \leqslant \nu_{0} + \nu_{0} \cdot t_{\text{obs}} \}$$
(1)
$$\rho_{n} = \{ h \in A_{k} \colon h \not\in B \land \nu_{0} - \nu_{0} \cdot t_{\text{obs}} \leqslant \nu_{h} \leqslant \nu_{0} + \nu_{0} \cdot t_{\text{obs}} \}.$$
(2)

3.2. Signal Distribution

Events and candidates were found using the turboSETI find_event method for all full cadences, which found a total of 43275 events and 651 candidates across all four bands. A breakdown of the results is summarized in Table 2. The drift rate, S/N, and frequency distribution of the hits and candidates detected at each band is shown in Figure 2. A sample of the plots of the candidate events is included in Appendix C.

L-band targets accounted for the largest share of hits (76%), while the X band amounts to the largest portion of hits among the remaining bands (15%), with the S and C bands accounting for 8% and 1% of total hits, respectively. We find that the L band accounts for 80% of total events, a slight increase compared to its hits proportion. Despite the S band comprising fewer hits than the X band, more events were recorded at the S band (13%) than at the X band (6%), whereas the relative proportion of C-band events remained unchanged throughout (1%). Overall, 17% of the total hits were present in candidate events—the hit—event conversion rate. ¹⁹ The L-band hit—event conversion rate was 18%, a low figure compared to those seen at the S (27%) and C bands (26%), which may indicate a stronger RFI presence. The proportion of candidates found at

the L band was significantly higher than was previously for hits, accounting for 97% of the total candidates. Table 3 gives an overview of these figures.

3.3. Event Groups

Following Price et al. (2020), events were grouped into event groups of 125 kHz frequency bins, in which the spacing between the highest and lowest start frequencies $\Delta\nu_{\rm event}$ in each bin was computed. From this value, the central frequency $\nu_{\rm event}$ for each event group was computed. The larger the cluster size, the greater the RFI (or technosignature) presence.

The candidate events at the *L* band were grouped into 135 frequency bins of 125 kHz, the lowest grouping at 1172 MHz and the highest at 1626 MHz.

The statistical variance (and thus, standard deviation σ) in frequency, S/N, and drift rate within an event group were found for each event group. A graphical depiction is shown in Appendix D. We define single sources of interference or technosignature as event groups whose events demonstrate uniformity in frequency, S/N, and drift rate, because signals that share similar characteristics are more likely to have a common origin. As such, we select event groups with $\sigma_{\nu} < 1$, $\sigma_{\text{S/N}} < 1$, and $\sigma_{\dot{\nu}} < 1$ as single sources. The results are shown in Table 4. Examples of single sources are in Appendix D.

The BL BLIMPY package (Breakthrough Listen Collaboration 2019) was used to produce diagnostic waterfall plots of the 20 single sources, in which upon visual inspection, interesting sources traceable to known RFI can be identified. A sample of these plots are included in Appendix D. All single-source event groups can be traced back to observations of five unique targets.

3.4. Transmitter Rate Limit

We can calculate the percentage of stars that could possess high duty cycle transmitters above the EIRP_{min} threshold, given

 $[\]overline{\ ^{19}}$ In general, the A - B conversion rate is A \rightarrow B = $\frac{total\ A}{total\ B},$ and, in context, roughly describes how much of A is contained in B.

our lack of detections. That is, of the stars observed at a particular band, the transmitter limit is the maximum proportion of those which possess narrowband transmitters. Values are computed using a one-sided Poisson confidence interval, assuming a conservative 50% probability of observing a signal, if present.

The transmitter rate limit was calculated at the L, S, C, and X bands, the results of which are presented in Table 2. Our transmitter limit of 12.72% indicates that fewer than 12.72% of the observed stars have putative transmitters operating in the range of 1–11 GHz.

A comparison of the derived transmitter rate limits to those of previous surveys is shown in Figure 3, where red, green, orange, and blue correspond to searches conducted at the L, S, C, and X bands, respectively. Our study provides similar constraints to previous studies, but over a much wider range of frequencies.

Although we calculate transmitter rates solely considering the TESS targets, the data set also includes significant "bycatch" of other stars (and, indeed, background galaxies) in the GBT pointings (see Wlodarczyk-Sroka et al. 2020). Hence additional constraints on the prevalence of more luminous transmitters at larger distances from Earth could in principle be calculated, in addition to those for the TESS targets presented here.

4. Conclusions

We report on the BL technosignature search of 28 stellar targets selected from the TIC identified as potential exoplanet hosts. Our observations spanning 1–11 GHz were searched for narrowband signals exhibiting drift rates within $\pm 4\,\mathrm{Hz}\,\mathrm{s}^{-1}$ above a minimum S/N threshold of 10, and no candidate signals unattributable to RFI were found. We derive an EIRP threshold of $4.9\times10^{14}\,\mathrm{W}$ and establish some of the deepest limits to date over such a wide band.

4.1. Future Work

BL is continuing to observe a larger sample of TOI targets. Furthermore, TESS has begun its extended mission and so will

continue to refine its TOI catalog,²⁰ enabling future SETI searches to have a larger number of confirmed, nearby exoplanets for study.

The Breakthrough Prize Foundation funds the Breakthrough Initiatives that manages Breakthrough Listen. The Green Bank Observatory facility is supported by the National Science Foundation, and is operated by Associated Universities, Inc. under a cooperative agreement. We thank the staff at Green Bank Observatory for their support with operations. R.T.was funded as a participant in the Berkeley SETI Research Center Research Experience for Undergraduates Site, supported by the National Science Foundation under grant No. 1950897.

We thank Richard Elkins and Luigi Cruz for help with development and debugging of turboSETI. We thank the referee for the helpful comments.

Software: turboSETI (Enriquez et al. 2017; Enriquez & Price 2019), BLIMPY (Breakthrough Listen Collaboration 2019), NUMPY (Harris et al. 2020), PANDAS (McKinney 2010; Pandas Development Team 2020), ASTROPY (Astropy Collaboration et al. 2013, 2018), DOCKER (Merkel 2014).

Appendix A turboSETI in the Google Cloud Platform

This work is the result of an endeavor to migrate the turboSETI pipeline onto the GCP (Figure 4). GCP Compute Engine instances were used to conduct the analysis instead of the compute nodes at the UC Berkeley Data Center. Each of the 20 instances were mounted to a GCS Bucket to access the fine-frequency resolution data products and installed with a containerized version of turboSETI as a DOCKER image to search for narrowband drifting signals. Five Compute Engines were assigned to analyze the data at each of the bands (*L*, *S*, *C*, and *X*). One of these instances acted as the head node and provided each Compute Engine a unique list of files to analyze. The head node then collected and searched the turboSETI raw output files for events. Events that passed turboSETI inspection were plotted.

https://tess.mit.edu/observations/

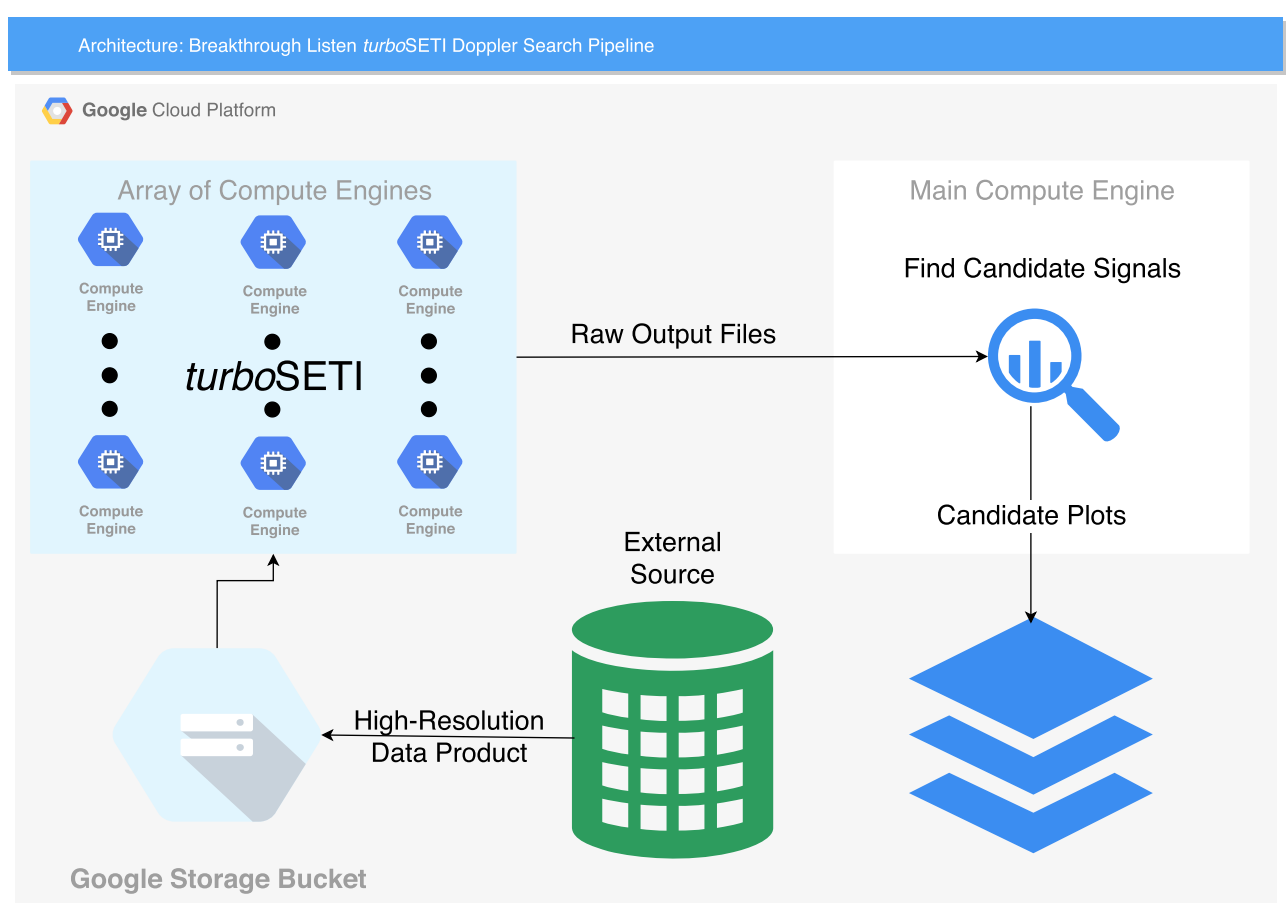


Figure 4. The turboSETI pipeline adapted for compatibility with the Google Cloud Platform.

Appendix B Targets

Table 5 presents the 28 targets studied in this work, which have been observed with the GBT at all four L, S, C, and X

bands. Each of the targets is present in the TOI catalog. Target data is sourced from the ExoFOP-TESS.

Table 5
Targets

TIC ID	TOI ID	R.A. (J2000)	Decl. (J2000)	Distance (pc)
154089169	1174.01	13:56:52.12	68:37:05.56	95
154840461	1153.01	12:10:45.97	85:42:18.28	147
154872375	1135.01	12:53:35.13	85:07:46.18	114
158002130	1180.01	14:18:13.39	82:11:37.55	72
159510109	1141.01	16:30:08.33	80:18:27.96	97
160268701	1143.01	12:10:09.28	77:21:08.15	192
198213332	1131.01	16:33:44.05	61:43:06.00	223
230088370	1176.01	16:29:25.60	71:30:21.14	296
232967666	1167.01	13:12:36.57	71:37:05.30	210
233087860	1184.01	18:08:49.08	60:40:43.62	59
266500992	1655.01	04:04:41.34	52:15:25.17	165
267489265	1132.01	19:55:07.51	54:46:53.20	287
267694283	1656.01	04:12:55.20	53:41:13.38	106
281731203	685.01	10:52:07.75	00:29:35.40	213
284450803	1142.01	19:22:50.15	56:36:55.39	299
287196418	1190.01	19:30:56.19	59:24:13.87	281
288185138	1200.01	14:51:21.94	82:57:08.13	224
289539327	1186.01	16:46:32.03	65:42:54.13	295
294176967	1170.01	20:03:13.23	52:02:27.03	880
302518439	1169.01	08:56:28.81	72:31:59.79	262
320525204	1140.01	17:39:50.77	56:04:44.30	123
341544930	1182.01	13:26:27.52	65:18:22.84	
349827430	1148.01	10:47:38.17	71:39:20.62	97
359496368	1178.01	18:36:24.25	55:23:30.41	37
372757221	1187.01	10:51:34.36	81:19:19.83	221
458478250	1165.01	15:28:35.19	66:21:31.35	126
459970307	1154.01	16:59:41.77	64:41:57.17	94
470315428	1673.01	04:18:35.64	52:51:54.12	472

Appendix C Examples of Candidate Events

There were 651 candidate events detected by turboSETI across all four bands. Figure 5 shows a candidate event found at each band. These events passed turboSETI inspection as

having signals with S/N > 10 present in the "ON" observations and none in the "OFF" observations. By visual inspection, it is easily verifiable that there are emissions of S/N < 10 present in "OFF" observations–characteristic of RFI. In this way, each of the 651 candidate events were rejected.

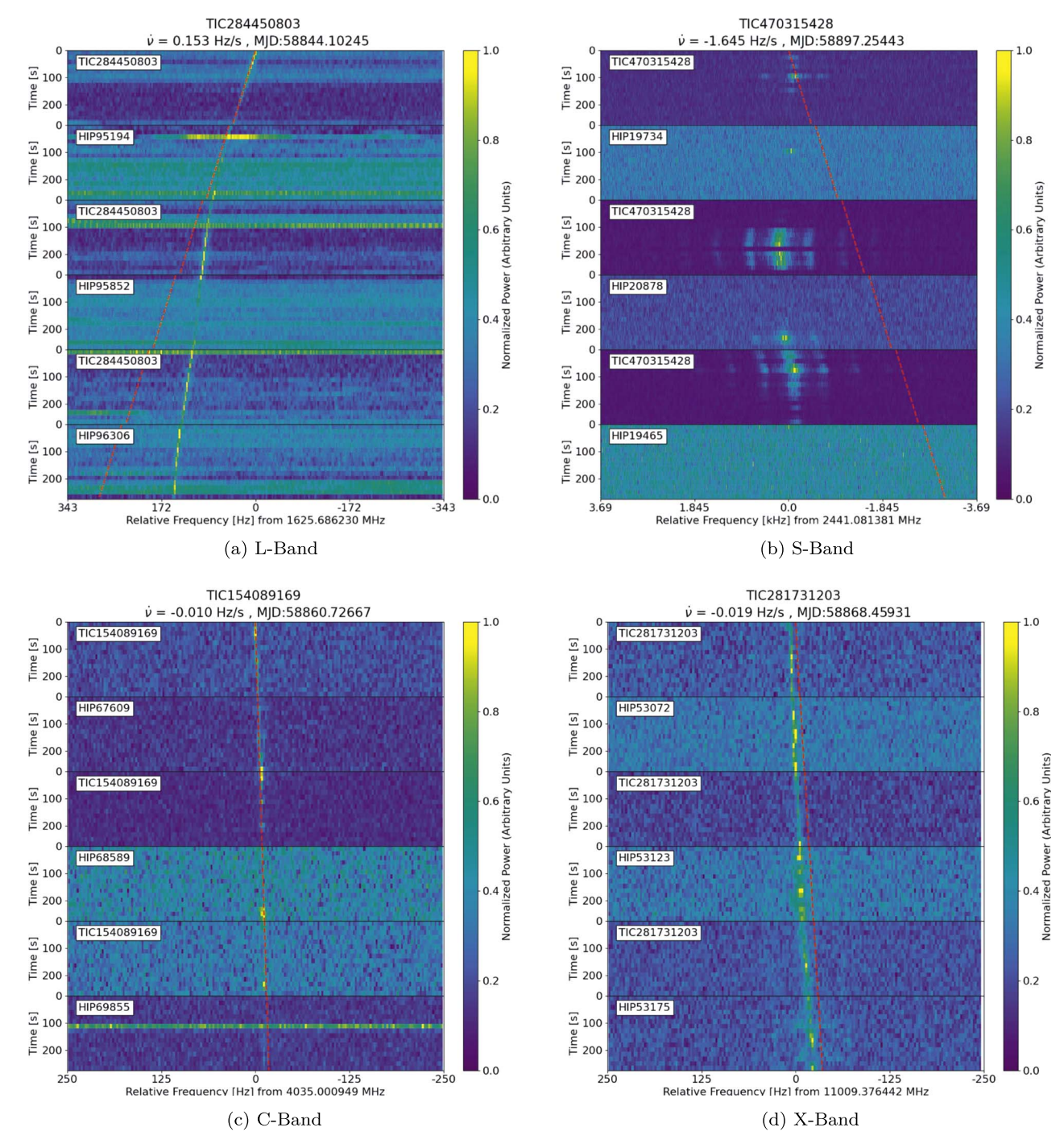


Figure 5. Spectra of events found by turboSETI found at each band. The panels are ordered sequentially following the "ON"—"OFF" observation cadence. The red dashed line indicates the drift rate computed by turboSETI for the first hit in the candidate event (although the underlying algorithm searches a range of drift for matches in the other five observations). Note that in cases such as Figures 5(a) and (b), the red line, assuming constant Doppler drift, is a poor match for the changing drift rate of the detected signal.

Appendix D Event Groups

Event groups are 125 kHz wide frequency ranges candidates that contain candidates identified by the turboSETI find_e-vent method. Since signals emanating from a single source are likely to be clustered in frequency and exhibit near-identical S/N and drift rates, we consider event groups possessing a

standard deviation less than 1 in frequency, S/N, and drift rate as single sources. The distribution of these variances is shown in Figure 6. In this way, technosignatures are those signals originating from single sources unattributable to RFI. There were no single-source signals that could not be attributed to RFI, but include sample plots of candidate technosignature sources shown in Figures 7 and 8. All single-source event groups are traceable to five unique targets.

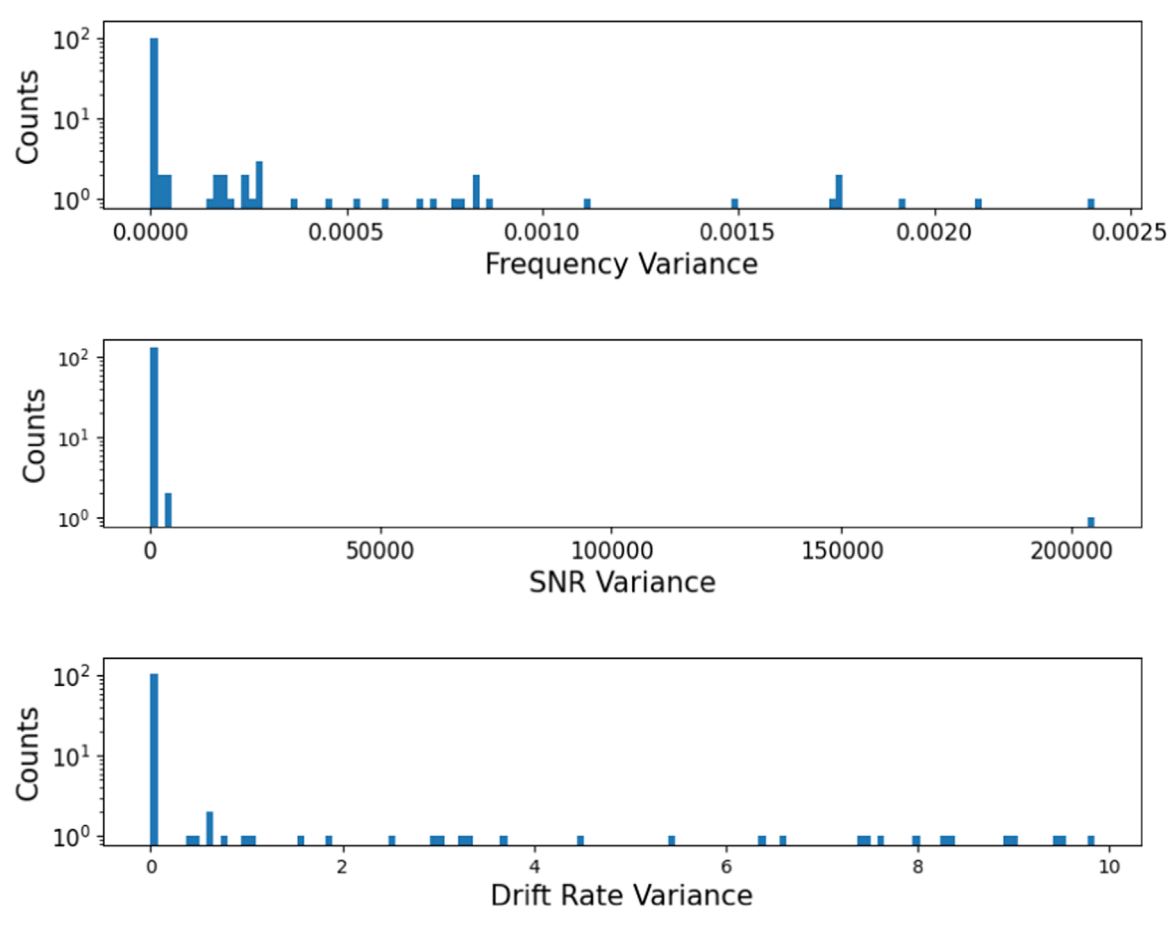


Figure 6. Histogram showing the variance of frequency, S/N, and drift rate of all event groups at the L band. All single-source events (events with a standard distribution $\sigma < 1$) for frequency, S/N, and drift rate, were found to exist only at the L band. We show the variance instead of the standard deviation since it is more effective in detecting outliers.

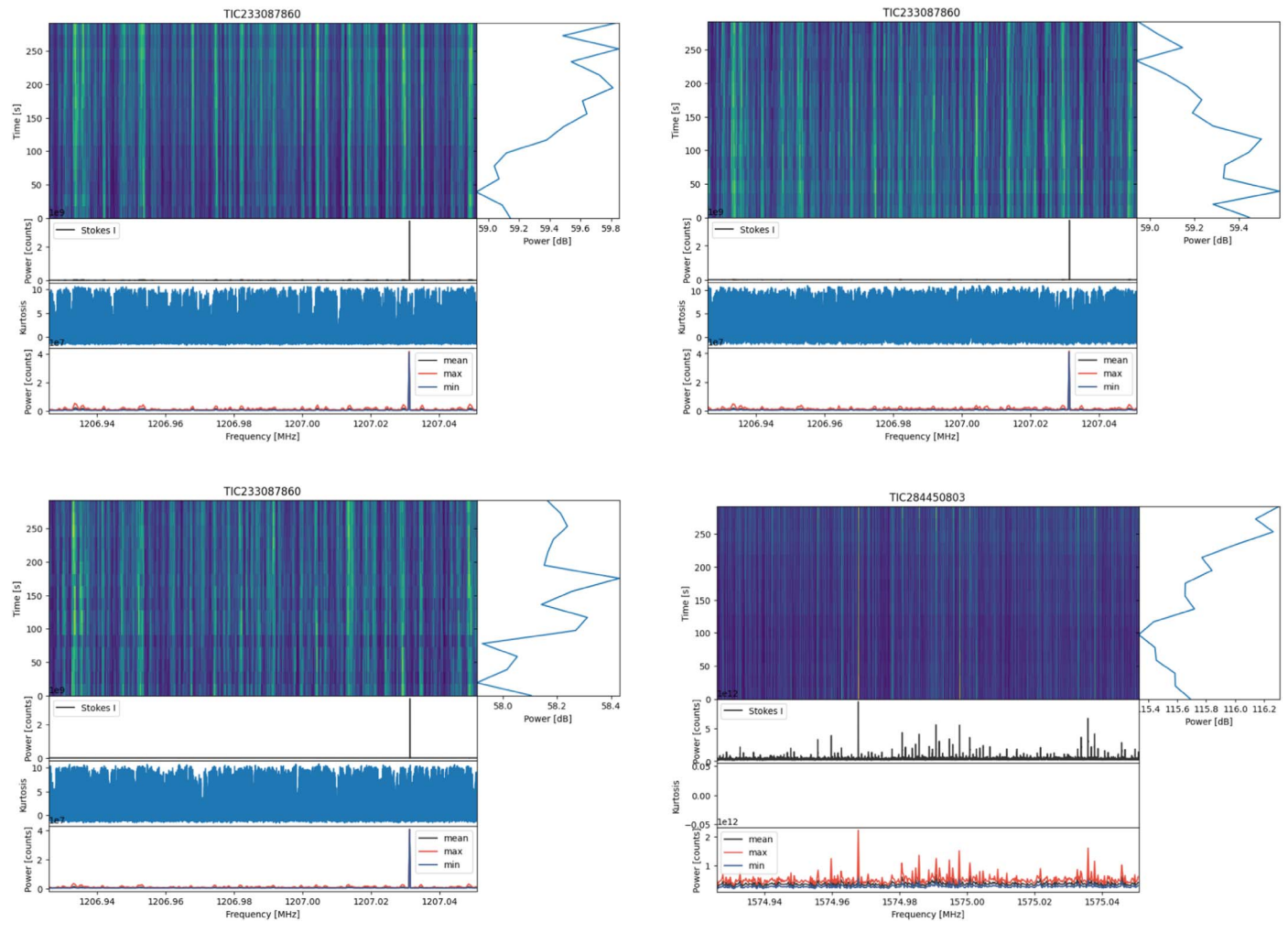


Figure 7. Examples of 125 kHz wide, *L*-band, single-source event groups traceable to observations of TIC233087860 and TIC284450803. Note how clustered signals exhibit nearly identical drift rates, S/N, and frequency. Note the frequencies shown are both present in navigation satellite bands, and these observations appear to be badly affected by RFI.

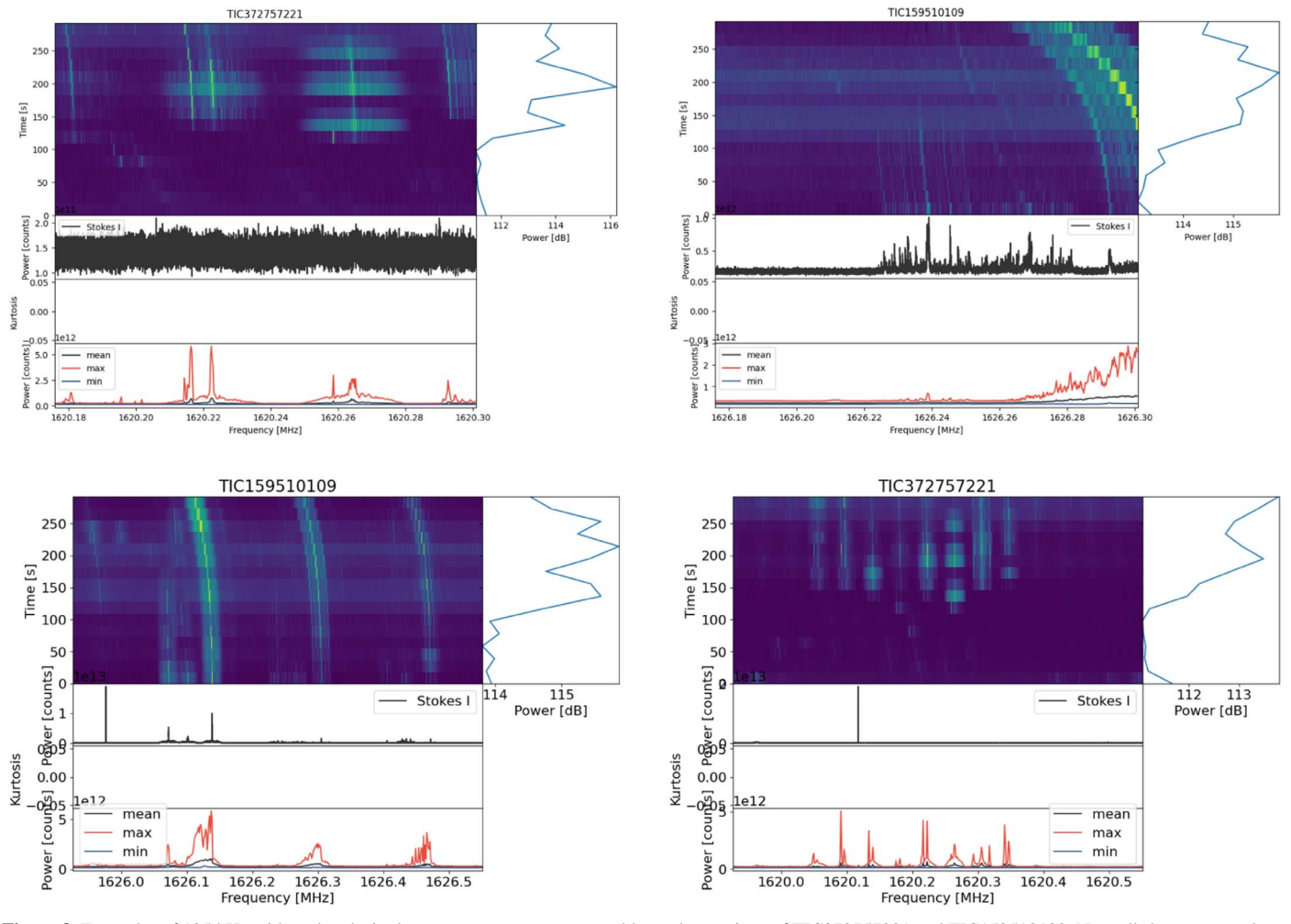


Figure 8. Examples of 125 kHz wide, L-band, single-source event groups traceable to observations of TIC372757221 and TIC159510109. Note all shown events have frequencies in the Iridium satellite band.

ORCID iDs

Raffy Traas https://orcid.org/0000-0002-3364-7009
Steve Croft https://orcid.org/0000-0003-4823-129X
Vishal Gajjar https://orcid.org/0000-0002-8604-106X
Howard Isaacson https://orcid.org/0000-0002-0531-1073
Matt Lebofsky https://orcid.org/0000-0002-7042-7566
Karen Perez https://orcid.org/0000-0002-6341-4548
Danny C. Price https://orcid.org/0000-0003-2783-1608
Sofia Sheikh https://orcid.org/0000-0001-7057-4999
Shane Smith https://orcid.org/0000-0003-4101-8234

References

Astropy Collaboration, Price-Whelan, A. M., SipHocz, B. M., et al. 2018, AJ, 156, 123

Astropy Collaboration, Robitaille, T. P., Tollerud, E. J., et al. 2013, A&A, 558, A33

Breakthrough Listen Collaboration 2019, Blimpy: Breakthrough Listen I/O Methods for Python, Astrophysics Source Code Library, ascl:1906.002

Brzycki, B., Siemion, A. P. V., Croft, S., et al. 2020, PASP, 132, 114501

Cocconi, G., & Morrison, P. 1959, Natur, 184, 844

Enriquez, E., & Price, D. 2019, turboSETI: Python-based SETI search algorithm, Astrophysics Source Code Library, ascl:1906.006

Enriquez, J. E., Siemion, A., Foster, G., et al. 2017, ApJ, 849, 104

Enriquez, J. E., Siemion, A., Lazio, T. J. W., et al. 2018, RNAAS, 2, 9

```
Gajjar, V., Perez, K., Siemion, A., et al. 2020, AJ, submitted (arXiv:2104.
   14148)
Gray, R. H., & Mooley, K. 2017, AJ, 153, 110
Harp, G. R., Richards, J., Tarter, J. C., et al. 2016, AJ, 152, 181
Harris, C. R., Millman, K. J., van der Walt, S. J., et al. 2020, Natur, 585,
   357
Horowitz, P., & Sagan, C. 1993, ApJ, 415, 218
Hsu, D. C., Ford, E. B., & Terrien, R. 2020, MNRAS, 498, 2249
Isaacson, H., Siemion, A. P. V., Marcy, G. W., et al. 2017, PASP, 129, 054501
Lacki, B. C., Brzycki, B., Croft, S., et al. 2020, arXiv:2006.11304
Lebofsky, M., Price, D. C., MacMahon, D. H., et al. 2019, PASP, 131, 124505
Lipman, D., Isaacson, H., Siemion, A. P. V., et al. 2019, PASP, 131, 034202
Margot, J.-L., Pinchuk, P., Geil, R., et al. 2021, AJ, 161, 55
McKinney, W. 2010, in Proc. 9th Python in Science Conference, ed.
   S. van der Walt & J. Millman (Austin, TX: SciPy), 56
Merkel, D. 2014, Linux Journal, 2014, 2
Pandas Development Team 2020, pandas-dev/pandas: Pandas, vlatest,
   Zenodo, doi:10.5281/zenodo.3509134
Perez, K., Brzycki, B., Gajjar, V., et al. 2020, RNAAS, 4, 97
Price, D. C., Enriquez, J. E., Brzycki, B., et al. 2020, AJ, 159, 86
Sheikh, S. Z. 2020, IJAsB, 19, 237
Sheikh, S. Z., Siemion, A., Enriquez, J. E., et al. 2020, AJ, 160, 29
Stassun, K. G., Oelkers, R. J., Paegert, M., et al. 2019, AJ, 158, 138
Tingay, S. J., Tremblay, C. D., & Croft, S. 2018, ApJ, 856, 31
Tremblay, C. D., & Tingay, S. J. 2020, PASA, 37, e035
Wlodarczyk-Sroka, B. S., Garrett, M. A., & Siemion, A. P. V. 2020, MNRAS,
   498, 5720
Worden, S. P., Drew, J., Siemion, A., et al. 2017, AcAau, 139, 98
```